ACS OMEGA

Open Access

http://pubs.acs.org/journal/acsodf

Article

Asymmetric and Skin-Mimicking Hydrogels with Wide Temperature Tolerance and Superior Elasticity for High-Performance Strain Sensors

Yunchao Xiao, Qinglong Chen, Zemeng Yang, Man Xi, Yili Zhao, Jianxun Fu, Yang Jiang,* and Yi Li*

Cite This: *ACS Omega* 2023, 8, 46676−46684

Read Online

ACCESS | Metrics & More | Article Recommendations

ABSTRACT: Wide temperature tolerance and superior mechanical properties are highly required for composite hydrogels in electronic applications such as electronic skins and soft robotics. In this work, a unique polyacrylamide-based and double-network hydrogel system is designed and fabricated by introducing graphene oxide and glycerol to improve mechanical properties as well as antifreezing and antiheating properties. Maximum stress of the graphene oxide-incorporated hydrogel increases rapidly to 500.0 kPa which is much higher than that of polymetric acrylamide/carboxymethylcellulose sodium hydrogel (281.7 kPa), probably due to the inhibition from graphene oxide in generation and propagation of cracks. With constantly adding glycerol, total elongation and antifreezing and heating properties of the composite hydrogels increase gradually. Especially, sample with 20 vol % of glycerol not only shows stable conductivity and wide temperature tolerance (−50 to 50 °C) but also has ideal strength-toughness match (597.6 kPa and 1263.4%), suggesting that synergistic effect of different layers in the asymmetric structure plays an active role in improvement of mechanical properties.

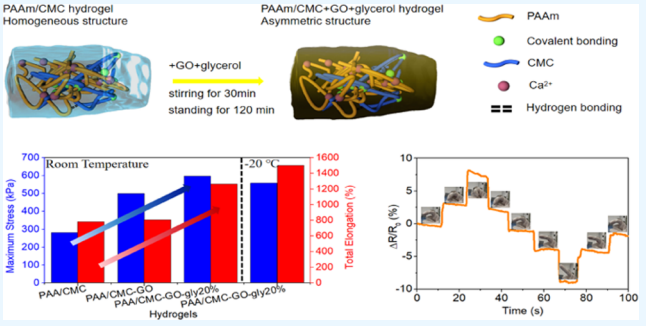

1. INTRODUCTION

Electronic skins (e-skins)[1−4] have aroused great attention of many scientists and been used in different applications such as artificial intelligence systems and wearable health care devices.[5−10] To simulate functions of real skins, it is essential for e-skins to have good mechanical properties, high conductivity, and antifreezing and antiheating properties. In recent years, hydrogels have been considered as one of the best candidates for preparation of e-skins owing to their tissue-mimicking features.[11,12] To endow hydrogels with high conductivity, inorganic nanofillers (such as metal ions[13,14] and nanomaterials[15]) have been employed to make e-skins respond to different stimuli rapidly.[16,17] This is the reason that e-skins have great potential in monitoring physiological signals and developing interactive robots with multiple functions.[18,19] According to many reports, output electronic signal of hydrogels can successfully change under tension or compression voice conditions.[20,21] To detect and collect weak signals, Bao's group recently designed and prepared a stretchable all-polymer light-emitting diode with high current efficiency, achieving signal transfer under low voltage and further promoting industrial application of e-skins.[22]

To date, skin-mimicking hydrogels have been developed based on both synthetic polymers and natural polymers. Among them, polyacrylamide (PAAm)-based hydrogels have shown great advantages due to their low price, ease of production, and good biocompatibility.[23,24] However, maximum stress of PAAm-based hydrogels were generally lower than 100 kPa,[23,25,26] which makes them difficult to use in applications that demand good mechanical properties. Many efforts have been made to improve mechanical properties of PAAm-based hydrogels. Gong's group first proposed construction of a double-network (DN) structure to effectively improve the maximum stress of hydrogels.[27] The DN structure consisted of a first network with good stiffness and a second network with good toughness, providing effective energy dissipation. Subsequently, many hydrogels including PAAm-based ones with DN structures were designed by using this mechanism and promoted to become good candidates for application.[28−31] Zheng et al. successfully prepared a DN hydrogel based on agar and PAAm by a one-pot method.[32] The DN agar/PAAm hydrogel showed a tensile strength of 1.0 MPa and a fraction strain of 2000%, while these values were

Received: August 7, 2023
Revised: October 6, 2023
Accepted: November 9, 2023
Published: November 27, 2023

only 0.3 MPa and ∼1800% for PAAm hydrogels. However, the DN structure for most hydrogels still had difficulty meeting requirements under high tension, which made multiple strengthen mechanism necessary. Introducing nanomaterials including carbon nanotubles (CNTs), silver nanowires (AgNWs), and graphene oxides (GO) into hydrogels can not only increase tensile stress, but also obtain excellent properties, such as mechanical properties and conductivity.[4,15,33]

Moreover, structures of previously reported e-skins and hydrogels were almost homogeneous,[31,34−36] showing only single strain mechanism during deformation. Inspired by building hierarchical microstructure of alloys to improve their tensile performance,[37] the asymmetric structure with different sublayers was designed and achieved collaboration between layers to adapt to deformation. Significantly, asymmetric structure is consistent with the real skin. What we all know is that skins are roughly divided into three layers: epidermis, dermis and subcutaneous tissue, and different layers play different roles. For example, epidermis provide good strength, while dermis has excellent toughness. In addition, real skins can work within a wide temperature ranging from −10 to 50 °C, which requests the e-skin to have antifreezing and antiheating properties.

In this work, a high-performance strain sensor with temperature tolerance was developed to face the challenges of PAAm-based e-skin, including low stress and loss of water. This work is mainly engaged in the following sections: First, a novel DN PAAm/carboxymethylcellulose (CMC) hydrogel incorporated with nanoscale GO was designed and prepared to increase the strength of the PAAm-based hydrogel. Then, the hydrogel was able to persistently work at both low and high temperatures after the addition of glycerol, owing to the fact that hydrogen bonding could improve the hydrogels' ability to lock water. In addition, an asymmetric structure simulating real skins was obtained by tuning the gradient distribution of GO under gravity, encouraging each layer to work in conjunction and improving the tensile performance of the hydrogel.

2. EXPERIMENTAL SECTION

2.1. Materials. Carboxymethylcellulose sodium (CMC, viscosity: 300−800 cP at room temperature) was supplied by Bioss (Beijing, China). Acrylamide (AAm, ≥99.0%), *N*,*N*′-methylenebis(acrylamide) (MBA, ≥99.0%), ammonium persulfate (APS, 99.0%), calcium chloride ($CaCl_2$, ≥96.0%), and glycerol were supplied by Tansole (Shanghai, China). GO was supplied by Guoheng Technology Co., Ltd. (Shenzhen, China). Deionized (DI) water was used in all experiments of this work.

2.2. Preparation of PAAm/CMC Hydrogels. The PAAm/CMC hydrogels were prepared by a one-pot method on the basis of the component ratios shown in Table 1. First, AAm, APS, and MBA were dissolved in 10 mL DI water in turn, followed by stirring the mixture for 30 min until a homogeneous and transparent solution was obtained. Then, CMC and $CaCl_2$ were added to the above solution followed by continuous stirring for another 10 min. The precursor solution was poured into a dumbbell-type mold with gauge length of 33 mm × 6 mm × 2 mm and polymerized at 60 °C for 60 min in an oven (Memmert UF260plus). The solid content of the hydrogels were set to 5, 8, 10, 13, 15, 18, and 20 wt %, respectively.

Table 1. Weight Ratio of Different Components in the Mixed Solution

component	AAm	APS	MBA	CMC	$CaCl_2$
ratio (wt %)	87.12	1.38	a little	9.20	2.30

According to the result, the hydrogel with 15% solid content was selected to study the change of structure and performances after addition of GO and glycerol. Specifically, 10 mg of GO was added to different volumes of DI water, and the mixture was ultrasonically vibrated for 10 min before addition of AAm. Finally, glycerol was injected into the above precursor solution, where 10 mL solvent with 0, 10, 20, 30 and 40 vol % glycerol was correspondingly named as PAAm/CMC-GO, PAAm/CMC-GO-$gly_{10\%}$, PAAm/CMC-GO-$gly_{20\%}$, PAAm/CMC-GO-$gly_{30\%}$ and PAAm/CMC-GO-$gly_{40\%}$. In addition, PAAm/CMC hydrogel was prepared as control (Table 2).

Table 2. Recipes for the PAAm/CMC Hydrogels

hydrogels	PAAm/CMC solid content (%)	GO (mg)	glycerol (mL)	DI water (mL)
PAAm/CMC	15	0	0	10
PAAm/CMC-GO	15	10	0	10
PAAm/CMC-GO-$gly_{10\%}$	15	10	1	9
PAAm/CMC-GO-$gly_{20\%}$	15	10	2	8
PAAm/CMC-GO-$gly_{30\%}$	15	10	3	7
PAAm/CMC-GO-$gly_{40\%}$	15	10	4	6

2.3. Swelling Measurement. Samples with diameters of 20 mm were immersed in beakers filled with DI water. Then, the weight (W) of each sample was measured. During the whole process, the ambient temperature and humidity were kept at 25 °C and 45%, respectively. In order to test swelling properties of the hydrogels, initial weight (W_0) of the samples were measured without drying process. The swelling diameter and weight ratios (Q) were calculated according to eq 1

$$Q = \frac{w - w_0}{w_0} \tag{1}$$

2.4. FTIR Measurement. The chemical structures of AAm, PAAm, CMC + $CaCl_2$ hydrogels and PAAm/CMC-GO-$gly_{20\%}$ were characterized using Fourier transform infrared spectrometer (FTIR, PerkinElmer Spectrum Two). The FTIR spectra were recorded in the spectral range of 1000−4000 cm^{-1} for each sample.

2.5. Morphology of the PAAm/CMC Hydrogels. Morphology of the PAAm/CMC hydrogels were observed using scanning electron microscope (SEM, Apero S HiVac) with a working current of 25 pA under an accelerating voltage of 2 kV. All samples were freeze-dried and then sputtered with gold for microscopic observation.

2.6. Mechanical Measurement. Uniaxial tensile tests were conducted using an Instron Tester 5882 tensile stage at room temperature, −20 and 50 °C with a speed of 80 mm/min. Rectangular dumbbell-shaped tensile specimens with a thickness of ∼2.00 mm were obtained in molds. For loading−unloading tests, stretching speeds of 80, 100, and 300 mm/min was used. Rectangular samples with a width of 20 mm and a thickness of 1.0 mm were used for the tests.

2.7. Rheological Measurement. Dynamic rheology performance of the hydrogels was performed on a DHR-2

https://doi.org/10.1021/acsomega.3c05779
ACS Omega 2023, 8, 46676−46684

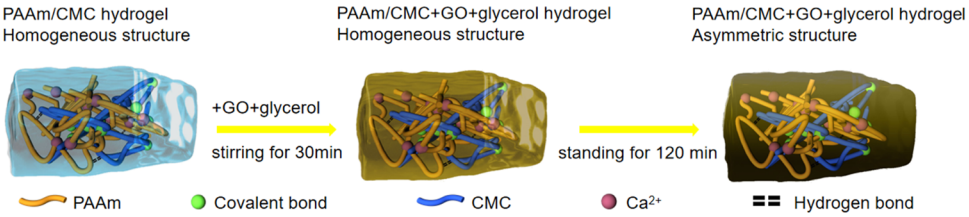

Figure 1. Schematic evolution diagram from the PAAm/CMC hydrogel to PAAm/CMC-GO-glycerol hydrogels with an asymmetric structure.

Table 3. Appearance of the PAAm/CMC Hydrogels with 5, 8, 10, 13, 15, 18 and 20% Solid Content

solid content	5, 8%	10, 13%	15, 16%	18, 20%
appearance of hydrogel	unstable lower strength	stable low strength	stable good toughness-strength match	stable toughness decreasing

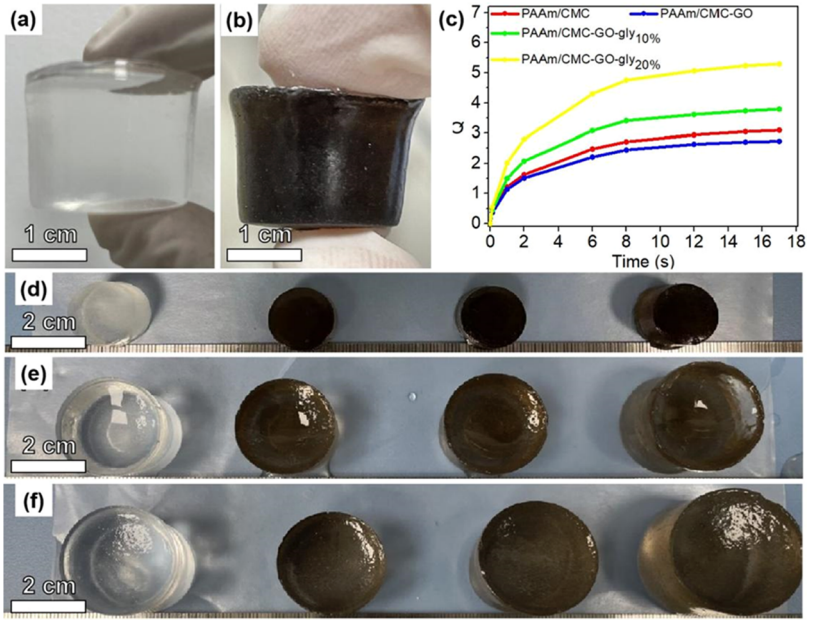

Figure 2. Images of (a) PAAm/CMC and (b) PAAm/CMC-GO-gly$_{20\%}$ hydrogels; Swelling curves (c) in 17 days of PAAm/CMC, PAAm/CMC-GO, PAAm/CMC-GO-gly$_{10\%}$ and PAAm/CMC-GO-gly$_{20\%}$ hydrogels and images on (d) day 0, (e) day 1, and (f) day 17. PAAm/CMC, PAAm/CMC-GO, PAAm/CMC-GO-gly$_{10\%}$ and PAAm/CMC-GO-gly$_{20\%}$ hydrogels are shown from left to right in (d–f).

Rheometer installed indenter with a diameter of 25 mm (TA DHR-2). For the frequency sweep test, the settled strain (γ) was 0.1%, and the frequency sweep was performed in a frequency range of 0.01−100 rad/s. For the strain scan test, the strain scan was performed at a fixed frequency of 10 rad/s in the strain range of 0.01−1000%.

2.8. Sensing Measurement. Sensing properties of the PAAm/CMC-GO-gly$_{20\%}$ hydrogel were demonstrated by combining a tensile tester and multimeter at different strains and speeds (KEITHLEY DMM75). The resistance changes of hydrogel during stretching were recorded by the multimeter. Likewise, sensing capacity of the hydrogels for monitoring human motion was also investigated using a multimeter. The hydrogels were attached on a human body directly, and both ends of the hydrogels were connected to the multimeter. The relative resistance variations were calculated by eq 2

$$\frac{\Delta R}{R_0} = \frac{R - R_0}{R_0} \times 100\% \tag{2}$$

wherein, R_0 and R were the representative of resistance of hydrogels before and after deforming.

2.9. Differential Scanning Calorimetry (DSC) Measurement. DSC (model: TA DSC250) was employed to analyze the low-temperature resistance of the hydrogels. The samples were placed in an airtight aluminum crucible before test with an empty crucible as reference. The initial temperature was −50 °C and gradually increased to 20 °C at a speed of 5 °C/min.

2.10. Antiheating Measurement. Antidrying capacity of the hydrogels were investigated at 50 °C. First, PAAm/CMC, PAAm/CMC-GO, PAAm/CMC-GO-gly$_{10\%}$, and PAAm/CMC-GO-gly$_{20\%}$ were shaped into discs and weighted (W'). Then, the samples were placed at 50 °C for 8 h, weighted again, and recorded as W_t. The water loss ratio (Q_W) of all hydrogels was calculated using eq 3

$$Q_W = \frac{W' - W_t}{W'} \tag{3}$$

3. RESULTS AND DISCUSSION

3.1. Structure Analysis of the PAAm/CMC Hydrogels. *3.1.1. Appearance and Swelling Property of the Hydrogels.* A DN hydrogel with good temperature tolerance is designed to

https://doi.org/10.1021/acsomega.3c05779
ACS Omega 2023, 8, 46676−46684

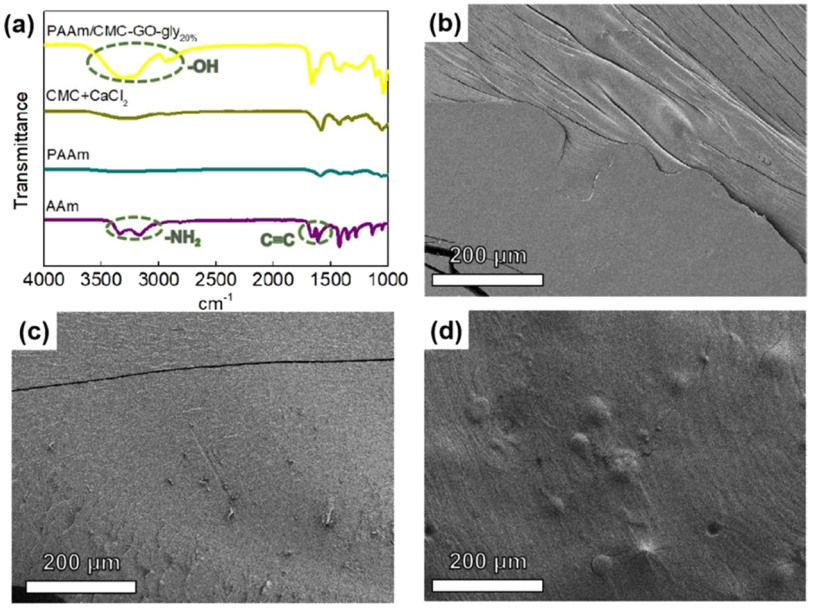

Figure 3. (a) FTIR spectra of AAm, PAAm, CMC + $CaCl_2$ and PAAm/CMC-GO-gly$_{20\%}$ hydrogels; typical SEM images of the top surface of (b) PAAm/CMC, (c) PAAm/CMC-GO, and (d) PAAm/CMC-GO-gly10% hydrogels after freeze-drying.

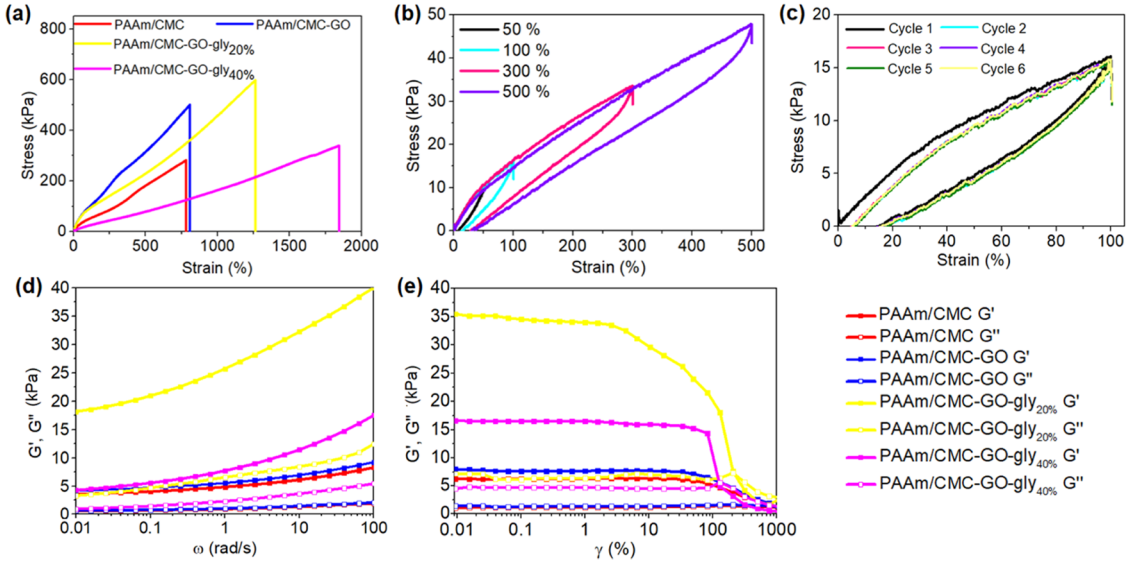

Figure 4. (a) Tensile stress−strain curves of PAAm/CMC, PAAm/CMC-GO, PAAm/CMC-GO-gly$_{20\%}$ and PAAm/CMC-GO-gly$_{40\%}$ hydrogels at room temperature; (b) different dissipated energy and the hysteresis curves of PAAm/CMC-GO-gly$_{20\%}$ hydrogel during loading and unloading cycles were studied (50, 100, 300, 500%); (c) six times continuing cyclic curves of PAAm/CMC-GO hydrogel at 100% strain and corresponding dissipated energy; dynamic rheological curves of PAAm/CMC, PAAm/CMC-GO, PAAm/CMC-GO-gly$_{20\%}$ and PAAm/CMC-GO-gly$_{30\%}$ hydrogels under (d) strain and (e) frequency, respectively.

obtain an ideal strength-toughness match by tuning the distribution of GO. APS and MBA were added to an AAm solution to initiate polymerization into PAAm and form a rigid network structure. The other flexible network structure was made of CMC + Ca^{2+} chelate, which was connected to the PAAm network through hydrogen bonding. GO displayed a gradient distribution under gravity and had an asymmetric structure in the hydrogel matrix, as shown in Figure 1.

Table 3 shows the appearance of PAAm/CMC hydrogels with different solid contents (SC). The appearance of samples with no more than 8 wt % SC exhibited instability, suggesting the strength of chemical network was weak. With SC increased to 10−20 wt %, the appearance of hydrogels became more stable, leading to a gradual increase in strength and decrease in toughness. The hydrogels with SC of 15 and 16 wt % displayed good strength and toughness, explaining the reason for choosing the SC of 15 wt % for further research in this work.

To clearly show the feasibility of the above design, the PAAm/CMC hydrogel and the PAAm/CMC hydrogel containing GO and 20 vol % of glycerol were prepared (Figure 2(a,b)). The former sample is transparent and homogeneous, while the latter one with GO and glycerol displayed gradient distribution of GO in the direction of gravity and has asymmetric structure, tallying with the predesign. Moreover, Figure 2(c) displays the weight ratio of PAAm/CMC, PAAm/CMC-GO, PAAm/CMC-GO-gly$_{10\%}$,

https://doi.org/10.1021/acsomega.3c05779
ACS Omega 2023, 8, 46676−46684

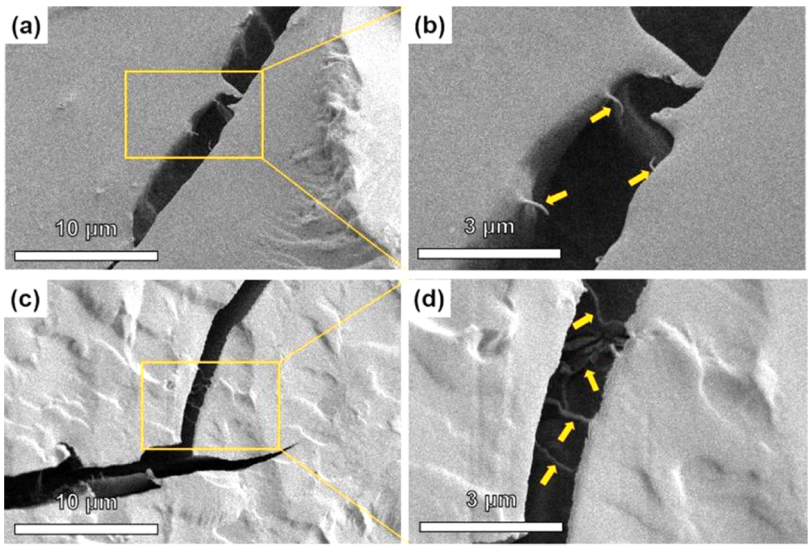

Figure 5. (a, c) Typical SEM morphology of tensile fracture-surface of the PAAm/CMC-GO hydrogel; (b, d) higher-magnification SEM images of PAAm/CMC-GO near cracks.

and PAAm/CMC-GO-gly$_{20\%}$ hydrogels during the swelling test. Values of Q rapidly increased in the beginning, and then became more and more slow until the slope was close to 0. Images recorded on day 0, day 1, and day 17 are provided in Figure 2(d−f), respectively. The diameter of the four samples became bigger and bigger, and this phenomenon is evident on the first day, which is consistent with the curves. Also, the weight ratio of the PAAm/CMC-GO hydrogel is lower than that of the PAAm/CMC hydrogel. However, with the increase of the volume fraction of glycerol, the change of the diameter and weight is more significant. The results suggest the cross-link indexes of PAAm/CMC and PAAm/CMC-GO hydrogels are higher than those of PAAm/CMC-GO-gly$_{10\%}$ and PAAm/CMC-GO-gly$_{20\%}$ hydrogels, due to the influence of hydrogen bonding.

3.1.2. Chemical Structure and Microstructure of the PAAm/CMC Hydrogels. To further determine the chemical structure of the PAAm/CMC hydrogels, FTIR was used to measure the AAm powder, PAAm, CMC+$CaCl_2$, and PAAm/CMC-GO-gly$_{20\%}$ hydrogels as shown in Figure 3(a). The FTIR spectroscopy of AAm (purple curve) displays typical characteristic absorption peaks of C═C (1680 and 1750 cm^{-1}) and −NH_2 (3201 and 3415 cm^{-1}). The C═C and −NH_2 peaks disappear in the cyan line, indicating that APS and MBA participated in the reaction with AAm. Moreover, the absorption peaks of PAAm/CMC-GO-gly$_{20\%}$ have no new complex peak except for a wide −OH (3,320 cm^{-1}) peak, suggesting that the PAAm/CMC hydrogels form a DN structure.

Figure 3(b−d) displays the morphology of PAAm/CMC, PAAm/CMC-GO, and PAAm/CMC-GO-gly$_{10\%}$ hydrogels, respectively. Compared to the other micropore surface in previous reports,[15,23] the surface of the PAAm/CMC hydrogel exhibits a smooth plane and a long fiber with cracks, due to lower solid content. After addition of GO, a rough plane and a few cracks are widely distributed on the hydrogel. Moreover, a rough plane and no obvious cracks are observed in PAAm/CMC-GO-gly$_{10\%}$ hydrogel under the combined effect of GO and glycerol.

3.2. Mechanical Properties of the PAAm/CMC Hydrogels at Room Temperature. *3.2.1. Tensile Performances of the PAAm/CMC Hydrogels.* Figure 4(a) shows tensile curves of the PAAm/CMC, PAAm/CMC-GO, PAAm/CMC-GO-gly$_{20\%}$, and PAAm/CMC-GO-gly$_{40\%}$ hydrogels. Both PAAm/CMC and PAAm/CMC-GO hydrogels without glycerol have similar total elongation (782.3 and 807.7%), but obvious difference in maximum stress (281.7 and 500.0 kPa). Compared with the mechanical properties of the PAAm/CMC-GO hydrogel, the total elongation and maximum stress of the PAAm/CMC-GO-gly$_{20\%}$ hydrogel rapidly go up to 1263.4 and 597.6 kPa. However, many literature studies[38−40] have reported that the stress of hydrogels with homogeneous composition gradually decreased as glycerol was constantly added. It is worth noting that the PAAm/CMC-GO-gly$_{20\%}$ hydrogel has an asymmetric structure that leads to different mechanical properties from those with homogeneous structure. To be specific, the layer with more GO makes the hydrogel undertake a great tension, and the one with less GO is helpful for total elongation, realizing that all layers work together and obtaining excellent strength toughness in the progress of tensile test. As the volume fraction of glycerol increases to 40%, the hydrogel shows a higher total elongation (1845.6%) but significantly decreased stress (339.0 kPa), which is closely related to the nondense network structure accepted by hydrogen bonding.

The fatigue resistance of the PAAm/CMC-GO-gly$_{20\%}$ hydrogel was studied by tensile cycle tests with different strains as shown in Figure 4(b). With the increase of tensile strain, hysteresis loops increase obviously, suggesting that the cross-linking points are severely damaged. Figure 4(c) displays the curves of 6 times of tensile cycles without residence time. The hysteresis curve and hysteresis energy of the following cycles are slightly lower than that of the first cycle but tend toward stability, indicating that the hydrogel containing GO and glycerol possesses fatigue resistance and rapid self-recovery.

3.2.2. Rheological Performances of the PAAm/CMC Hydrogels at Room Temperature. To reveal the microscopic mechanical performance of hydrogels after introducing GO and glycerol, their dynamic storage modulus (G') and loss modulus (G'') are measured with different frequency sweeps in Figure 4(d). Both G' and G'' values of the PAAm/CMC-GO

https://doi.org/10.1021/acsomega.3c05779
ACS Omega 2023, 8, 46676−46684

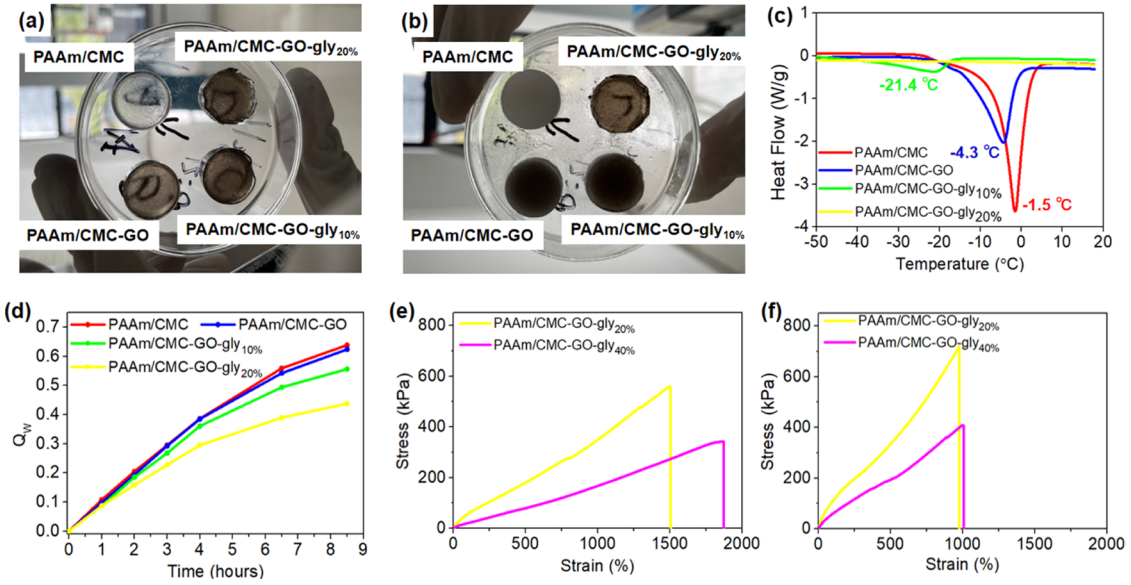

Figure 6. Antifreezing images of PAAm/CMC, PAAm/CMC-GO, PAAm/CMC-GO-gly$_{10\%}$ and PAAm/CMC-GO-gly$_{20\%}$ hydrogels testing at −25 °C for (a) 0 day and (b) 8 day; (c) DSC measurements in the range from −50 to 20 °C; (d) antiheating curves at 50 °C in 8.5 h; tensile stress−strain curves of PAAm/CMC-GO-gly$_{20\%}$ and PAAm/CMC-GO-gly$_{40\%}$ hydrogels (e) at −20 °C and (f) at 50 °C.

hydrogel are higher than those of the PAAm/CMC hydrogel over the entire frequency range. Also, both hydrogels show the same result that G' is much higher than G'' over the frequency range, which is identical with the solid-like, elastic nature of hydrogels. In addition, the values of G' and G'/G'' dramatically increase for the PAAm/CMC-GO-gly$_{20\%}$ hydrogel, attributed to the strong interface interaction from asymmetric structure. G' and G'' values decrease gradually as the volume fraction of glycerol rises, which is consistent with tensile loading−unloading tests. A significant strain-dependent viscoelastic response for all samples could be observed in the curves (Figure 4(e)) for G' and G'' as a function of shear strain (γ). In the linear viscoelastic region of γ from 0.1 to 10%, the G' and G'' of PAAm/CMC-GO-gly$_{20\%}$, PAAm/CMC-GO-gly$_{30\%}$, PAAm/CMC-GO, and PAAm/CMC hydrogels decrease in sequence, suggesting that an appropriate content of glycerol and GO is capable of effectively optimizing mechanical performances. However, the hydrogels exhibit slop-droop nonlinear viscoelastic behavior at an else shear strain range from 10 to 1000%, and the modulus of the hydrogels without glycerol decreases slowly. This phenomenon indicates that the DN incorporation is easily induced by the shear strain.

3.2.3. Microstructure of the PAAm/CMC-GO Hydrogel Near Cracks Generated by the Tensile Process. Figure 5(a,c) presents typical SEM images showing the tensile fracture-surface morphology of the PAAm/CMC-GO hydrogel. Some whiskers are observed in cracks that are scattered in the plane and short fiber-shaped region. To reveal the clear morphology of whiskers, the higher-magnification SEM images taken from the region marked in Figure 5(a,c) are displayed in Figure 5(b,d), respectively. The nanoscale GO that the orange arrows point out sew up the cracks like a thread, leading to improved strength of the hydrogels.

3.3. Temperature-Tolerance Performance and Mechanical Properties of PAAm/CMC Hydrogels. *3.3.1. Antifreezing and Antiheating Performances of the PAAm/CMC, PAAm/CMC-GO, PAAm/CMC-GO-gly$_{10\%}$, and PAAm/CMC-GO-gly$_{20\%}$ Hydrogels.* To preliminarily understand the antifreezing properties of the hydrogels, PAAm/CMC, PAAm/CMC-GO, PAAm/CMC-GO-gly$_{10\%}$, and PAAm/CMC-GO-gly$_{20\%}$ hydrogels are placed in a refrigerator at −25 °C for 8 days, as shown in Figure 6(a,b). It is observed that the PAAm/CMC-GO-gly$_{20\%}$ hydrogel still keeps its original state, while others are frozen after 8 days. To further explore the antifreezing performance, the crystallization temperature of the hydrogels is determined by DSC analysis. As shown in Figure 6(c), the crystallization peak temperatures of PAAm/CMC and PAAm/CMC-GO hydrogels are −1.5 and −4.3 °C, respectively. The crystallization peak temperature of the hydrogel is −21.4 °C after addition of 10 vol % glycerol, due to the addition of hydrogen bond lowering their crystallization temperature. As the volume fraction of glycerol reaches 20 vol %, the temperature drops to below −50 °C, and the result was consistent with the phenomenon shown in Figure 6(a,b).

It is difficult for most hydrogels to avoid water loss at room temperature or elevated temperature, restricting further application of the materials. A universal and effective way to solve this problem is introducing hydrogen bonding, which can be damaged under continuously absorbing energy and is finally helpful to slow down evaporation. The curves of Q_W at 50 °C are shown in Figure 6(d) and used to display the antiheating performance of all hydrogels. Compared with the hydrogels without glycerol, the Q_W value of the PAAm/CMC-GO-gly$_{10\%}$ hydrogel is lower, suggesting that glycerol has a positive effect on preventing evaporation. As glycerol increases to 20 vol %, the Q_W value further decreases.

3.3.2. Tensile Performance of PAAm/CMC-GO-gly$_{20\%}$ and PAAm/CMC-GO-gly$_{40\%}$ Hydrogels at Low and High Temperatures. According to the above results, PAAm/CMC-GO-gly$_{20\%}$ and PAAm/CMC-GO-gly$_{40\%}$ hydrogels are chosen to study antifreezing and antiheating properties since the other samples are difficult to be applied in lower or higher temperature. Furthermore, Figure 6(e,f) displays the tensile testing curves of the two hydrogels at −20 and 50 °C, respectively. Compared with the same samples at room temperature shown in Figure 4(a), the total elongation and maximum stress of the PAAm/CMC-GO-gly$_{20\%}$ (1503.7%,

https://doi.org/10.1021/acsomega.3c05779
ACS Omega 2023, 8, 46676−46684

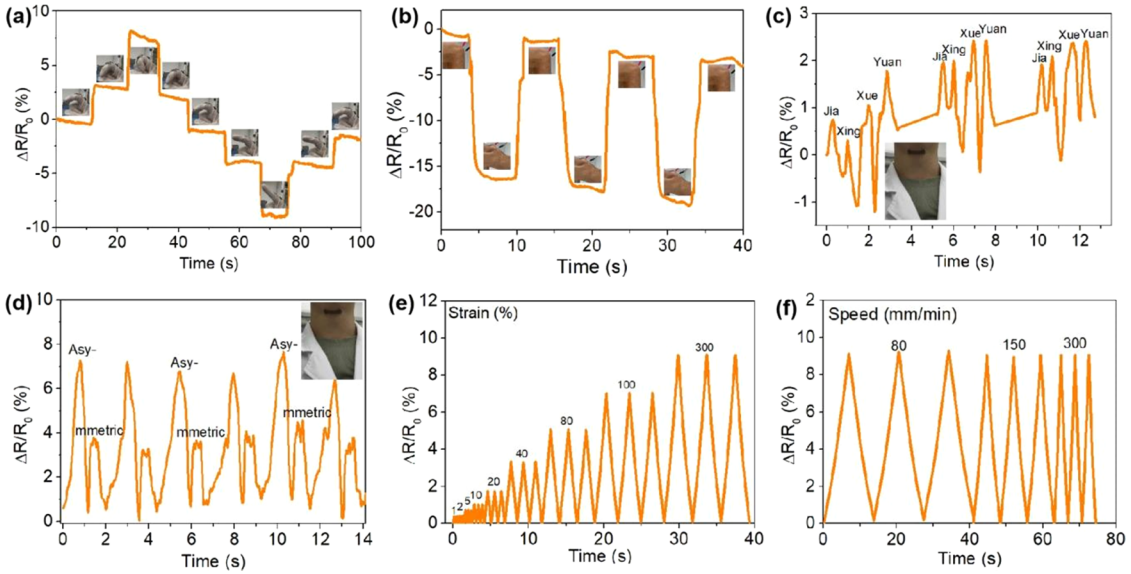

Figure 7. Resistance variation of PAAm/CMC-GO-gly$_{20\%}$ hydrogel responds to the different bending angles of (a) knuckle; (b) knee; (c, d) detection of speaking when the hydrogel mounts on throat. Relative resistance of PAAm/CMC-GO-gly$_{20\%}$ changes in response to (e) the tensile strain varied from 1 to 300% and (f) the tensile speed of 80, 150, and 300 mm/min.

558.5 kPa) and PAAm/CMC-GO-gly$_{40\%}$ (1874.1%, 342.3 kPa) hydrogels show no significant change at −20 °C, indirectly confirming that glycerol is helpful to reduce crystallization temperature. When PAAm/CMC-GO-gly$_{20\%}$ and PAAm/CMC-GO-gly$_{40\%}$ hydrogels are tested at 50 °C, the total elongations of PAAm/CMC-GO-gly$_{20\%}$ and PAAm/CMC-GO-gly$_{40\%}$ hydrogels fall (975.0 and 1009.5%), while the maximum stress rises (719.6 and 403.6 kPa), due to the fact that losing water makes the double-network structure become denser, and the hydrogels still keep good strength-toughness match and are still applied.

3.4. Sensing Properties of PAAm/CMC-GO-gly$_{20\%}$.

Based on the overall performances of real skin with good mechanical properties, stable conductivity, and outstanding sensitivity, the PAAm/CMC-GO-gly$_{20\%}$ hydrogel simulating real skin has enormous potential for monitoring various human motions. As shown in Figure 7(a,b), the relative resistance changes ($\Delta R/R_0$) of the hydrogel covering the knuckle and knee show the corresponding regular changes with a reciprocating joint bending angle, which is caused by the length and cross-section area fluctuation of the hydrogel during the joint movement. Furthermore, the hydrogel transducer possesses the ability of speech recognition; for instance, different current signal patterns could be detected when the tester uttered different voices such as "Jia", "Xing", "Xue", "Yuan", and "Asymmetric"; thus, the hydrogel sensor could be used for language rehabilitation and recognition of language-disabled people (Figure 7(c,d)).

Figure 7(e,f) shows the $\Delta R/R_0$ of PAAm/CMC-GO-gly$_{20\%}$ hydrogel at different tensile strains (1−300%) and speed (80−300 mm/min), respectively. The repeatable and stable signals could be monitored under different strains and speed. Especially, the hydrogel is extremely sensitive to both small strain and fast speed, and superb reliability is exhibited during the repeated stretching-produced stable output signals.

4. CONCLUSIONS

In this work, novel asymmetric and conductive PAAm-based hydrogels were designed, and their structure and multiple properties were studied and discussed. First, PAAm/CMC hydrogels with 15% and 16% solid contents show a DN structure and smooth surface with cracks after cold-drying. The morphology of the hydrogels is rough with few cracks after introducing GO/glycerol. Second, the maximum stress of the PAAm/CMC-GO hydrogel increases to 500 kPa, which is much higher than that of the PAAm/CMC hydrogel (281.7 kPa), while both are low in total elongation. The PAAm/CMC-GO-gly$_{20\%}$ not only has outstanding total elongation (1263.4%) after addition of 20 vol % glycerol, but also shows a higher stress (597.6 kPa), due to the asymmetric structure and suture function from GO. With further increase in the content of glycerol, the maximum stress of PAAm/CMC-GO-gly$_{40\%}$ decreases to 339.0 kPa. In addition, the crystallization temperature of the samples gradually decreases from −21 °C to below −50 °C as the volume fraction of glycerol increases from 10 to 20%. As for the PAAm/CMC-GO-gly$_{20\%}$ hydrogel, for one thing, the total elongation and maximum stress reach to 975% and 719.6 kPa at 50 °C, respectively. For another, the hydrogel shows stable conductivity and outstanding sensitivity on monitoring small changes in the process of tensile test and various human motions and small tensile stress. In summary, the PAAm/CMC hydrogels have great capability to be used as a strain sensor for detecting subtle strain changes over a wide temperature range.

■ ASSOCIATED CONTENT

Data Availability Statement

Data will be made available on request.

■ AUTHOR INFORMATION

Corresponding Authors

Yang Jiang − *College of Materials and Textile Engineering, Jiaxing University, Jiaxing 314001 Zhejiang, China;* orcid.org/0000-0002-9443-3696; Email: jiangyang1981@zjxu.edu.cn

Yi Li − *College of Materials and Textile Engineering, Jiaxing University, Jiaxing 314001 Zhejiang, China;* orcid.org/0000-0002-0635-7639; Email: liyi@zjxu.edu.cn

https://doi.org/10.1021/acsomega.3c05779
ACS Omega 2023, 8, 46676−46684

Authors

Yunchao Xiao − *College of Materials and Textile Engineering, Jiaxing University, Jiaxing 314001 Zhejiang, China;* orcid.org/0000-0002-8737-8027

Qinglong Chen − *College of Materials and Textile Engineering, Jiaxing University, Jiaxing 314001 Zhejiang, China*

Zemeng Yang − *College of Materials and Textile Engineering, Jiaxing University, Jiaxing 314001 Zhejiang, China*

Man Xi − *College of Materials and Textile Engineering, Jiaxing University, Jiaxing 314001 Zhejiang, China*

Yili Zhao − *College of Materials and Textiles, Zhejiang Sci-Tech University, Hangzhou 310018, China*

Jianxun Fu − *School of Materials Science and Engineering, Shanghai University, Shanghai 200444, China*

Complete contact information is available at: https://pubs.acs.org/10.1021/acsomega.3c05779

Author Contributions

Y.J. and Y.L. provided the conception and experimental design of this work. Y.C.X. and Z.M.Y. conducted the experiments and measurements. Q.L.C., M.X., Y.L.Z., and J.X.F. carried out result analysis and revised the manuscript. All authors discussed the results and commented on the manuscript.

Notes

The authors declare no competing financial interest.

There is no Supporting Information related to this article.

This work was not involved in human tissue or any other animal experiments.

■ ACKNOWLEDGMENTS

This work was supported by the Zhejiang Provincial Natural Science Foundation (LY22E030012; LQ22C100002), Science and Technology Bureau of Jiaxing City (2021AY10056; 2023AD11042), Key Laboratory of Yarn Materials Forming and Composite Processing Technology, Zhejiang Province (70722003-2207), and National Natural Science Foundation of China (NSFC) (No. 81901900).

■ REFERENCES

(1) Guo, H.; Han, Y.; Zhao, W.; Yang, J.; Zhang, L. Universally autonomous self-healing elastomer with high stretchability. *Nat. Commun.* **2020**, *11* (1), No. 2037, DOI: 10.1038/s41467-020-15949-8.

(2) Rao, J.; Chen, Z.; Zhao, D.; Ma, R.; Yi, W.; Zhang, C.; Liu, D.; Chen, X.; Yang, Y.; Wang, X.; Wang, J.; Yin, Y.; Wang, X.; Yang, G.; Yi, F. Tactile electronic skin to simultaneously detect and distinguish between temperature and pressure based on a triboelectric nanogenerator. *Nano Energy* **2020**, *75*, No. 105073.

(3) Zhou, K.; Zhao, Y.; Sun, X.; Yuan, Z.; Zheng, G.; Dai, K.; Mi, L.; Pan, C.; Liu, C.; Shen, C. Ultra-stretchable triboelectric nanogenerator as high-sensitive and self-powered electronic skins for energy harvesting and tactile sensing. *Nano Energy* **2020**, *70*, No. 104546.

(4) Gong, S.; Zhang, B.; Zhang, J.; Wang, Z. L.; Ren, K. Biocompatible poly(lactic acid)-based hybrid piezoelectric and electret nanogenerator for electronic skin applications. *Adv. Funct. Mater.* **2020**, *30* (14), No. 1908724, DOI: 10.1002/adfm.201908724.

(5) Xia, S.; Song, S.; Li, Y.; Gao, G. Highly sensitive and wearable gel-based sensors with a dynamic physically cross-linked structure for strain-stimulus detection over a wide temperature range. *J. Mater. Chem. C* **2019**, *7* (36), 11303−11314.

(6) Bai, J.; Wang, R.; Wang, X.; Liu, S.; Wang, X.; Ma, J.; Qin, Z.; Jiao, T. Biomineral calcium-ion-mediated conductive hydrogels with high stretchability and self-adhesiveness for sensitive iontronic sensors. *Cell Rep. Phys. Sci.* **2021**, *2* (11), No. 100623.

(7) Zhu, Y.; Liu, J.; Guo, T.; Wang, J. J.; Tang, X.; Nicolosi, V. Multifunctional Ti3C2Tx MXene Composite Hydrogels with Strain Sensitivity toward Absorption-Dominated Electromagnetic-Interference Shielding. *ACS Nano* **2021**, *15* (1), 1465−1474.

(8) Li, F.; Liu, Y.; Shi, X.; Li, H.; Wang, C.; Zhang, Q.; Ma, R.; Liang, J. Printable and Stretchable Temperature-Strain Dual-Sensing Nanocomposite with High Sensitivity and Perfect Stimulus Discriminability. *Nano Lett.* **2020**, *20* (8), 6176−6184.

(9) Ma, X.; Wang, C.; Wei, R.; He, J.; Li, J.; Liu, X.; Huang, F.; Ge, S.; Tao, J.; Yuan, Z.; Chen, P.; Peng, D.; Pan, C. Bimodal Tactile Sensor without Signal Fusion for User-Interactive Applications. *ACS Nano* **2022**, *16* (2), 2789−2797.

(10) Khatib, M.; Zohar, O.; Saliba, W.; Haick, H. A Multifunctional Electronic Skin Empowered with Damage Mapping and Autonomic Acceleration of Self-Healing in Designated Locations. *Adv. Mater.* **2020**, *32* (17), No. 2000246, DOI: 10.1002/adma.202000246.

(11) Mukhopadhyay, A.; Rajput, M.; Barui, A.; Chatterjee, S. S.; Pal, N. K.; Chatterjee, J.; Mukherjee, R. Dual cross-linked honey coupled 3D antimicrobial alginate hydrogels for cutaneous wound healing. *Mater. Sci. Eng., C* **2020**, *116*, No. 111218.

(12) Li, X.; Hetjens, L.; Wolter, N.; Li, H.; Shi, X.; Pich, A. Charge-reversible and biodegradable chitosan-based microgels for lysozyme-triggered release of vancomycin. *J. Adv. Res.* **2023**, *43*, 87−96.

(13) Chen, H.; Gao, Y.; Ren, X.; Gao, G. Alginate fiber toughened gels similar to skin intelligence as ionic sensors. *Carbohydr. Polym.* **2020**, *235*, No. 116018.

(14) Gao, Z.; Li, Y.; Shang, X.; Hu, W.; Gao, G.; Duan, L. Bioinspired adhesive and self-healing hydrogels as flexible strain sensors for monitoring human activities. *Mater. Sci. Eng., C* **2020**, *106*, No. 110168.

(15) Kim, S. K.; Lee, G. H.; Jeon, C.; Han, H. H.; Kim, S. J.; Mok, J. W.; Joo, C. K.; Shin, S.; Sim, J. Y.; Myung, D.; Bao, Z.; Hahn, S. K. Bimetallic Nanocatalysts Immobilized in Nanoporous Hydrogels for Long-Term Robust Continuous Glucose Monitoring of Smart Contact Lens. *Adv. Mater.* **2022**, *34* (18), No. 2110536, DOI: 10.1002/adma.202110536.

(16) Lu, Y.; Luo, Q.; Jia, X.; Tam, J. P.; Yang, H.; Shen, Y.; Li, X. Multidisciplinary strategies to enhance therapeutic effects of flavonoids from Epimedii Folium: Integration of herbal medicine, enzyme engineering, and nanotechnology. *J. Pharm. Anal.* **2023**, *13* (3), 239−254.

(17) Li, X.; Gao, Y.; Li, H.; Majoral, J.-P.; Shi, X.; Pich, A. Smart and bioinspired systems for overcoming biological barriers and enhancing disease theranostics. *Prog. Mater. Sci.* **2023**, *140*, No. 101170, DOI: 10.1016/j.pmatsci.2023.101170.

(18) Kim, H. J.; Sim, K.; Thukral, A.; Yu, C. Rubbery electronics and sensors from intrinsically stretchable elastomeric composites of semiconductors and conductors. *Sci. Adv.* **2017**, *3*, No. e1701114, DOI: 10.1126/sciadv.1701114.

(19) Wang, S.; Xu, J.; Wang, W.; Wang, G.-J. N.; Rastak, R.; Molina-Lopez, F.; Chung, J. W.; Niu, S.; Feig, V. R.; Lopez, J.; Lei, T.; Kwon, S.-K.; Kim, Y.; Foudeh, A. M.; Ehrlich, A.; Gasperini, A.; Yun, Y.; Murmann, B.; Tok, J. B. H.; Bao, Z. Skin electronics from scalable fabrication of an intrinsically stretchable transistor array. *Nature* **2018**, *555* (7694), 83−88.

(20) Hua, Q.; Sun, J.; Liu, H.; Bao, R.; Yu, R.; Zhai, J.; Pan, C.; Wang, Z. L. Skin-inspired highly stretchable and conformable matrix networks for multifunctional sensing. *Nat. Commun.* **2018**, *9* (1), No. 244, DOI: 10.1038/s41467-017-02685-9.

(21) Kang, S.; Cho, S.; Shanker, R.; Lee, H.; Park, J.; Um, D.-S.; Lee, Y.; Ko, H. Transparent and conductive nanomembranes with orthogonal silver nanowire arrays for skin-attachable loudspeakers and microphones. *Sci. Adv.* **2018**, *4*, No. eaas8772, DOI: 10.1126/sciadv.aas8772.

(22) Zhang, Z.; Wang, W.; Jiang, Y.; Wang, Y.-X.; Wu, Y.; Lai, J.-C.; Niu, S.; Xu, C.; Shih, C.-C.; Wang, C.; Yan, H.; Galuska, L.; Prine, N.; Wu, H.-C.; Zhong, D.; Chen, G.; Matsuhisa, N.; Zheng, Y.; Yu, Z.;

Wang, Y.; Dauskardt, R.; Gu, X.; Tok, J. B. H.; Bao, Z. High-brightness all-polymer stretchable LED with charge-trapping dilution. *Nature* **2022**, *603* (7902), 624−630.
(23) Gao, Y.; Jia, F.; Gao, G. Transparent and conductive amino acid-tackified hydrogels as wearable strain sensors. *Chem. Eng. J.* **2019**, *375*, No. 121915.
(24) Gao, Y.; Gu, S.; Jia, F.; Wang, Q.; Gao, G. All-in-one" hydrolyzed keratin protein-modified polyacrylamide composite hydrogel transducer. *Chem. Eng. J.* **2020**, *398*, No. 125555.
(25) Liu, X.; Zhang, Q.; Gao, G. DNA-inspired anti-freezing wet-adhesion and tough hydrogel for sweaty skin sensor. *Chem. Eng. J.* **2020**, *394*, No. 124898.
(26) Xu, J.; Jin, R.; Ren, X.; Gao, G. A wide temperature-tolerant hydrogel electrolyte mediated by phosphoric acid towards flexible supercapacitors. *Chem. Eng. J.* **2021**, *413*, No. 127446.
(27) Gong, J. P.; Katsuyama, Y.; Kurokawa, T.; Osada, Y. Double-Network Hydrogels with Extremely High Mechanical Strength. *Adv. Mater.* **2003**, *15* (14), 1155−1158.
(28) Peng, W.; Han, L.; Huang, H.; Xuan, X.; Pan, G.; Wan, L.; Lu, T.; Xu, M.; Pan, L. A direction-aware and ultrafast self-healing dual network hydrogel for a flexible electronic skin strain sensor. *J. Mater. Chem. A* **2020**, *8* (48), 26109−26118.
(29) Zhang, J.; Qian, S.; Chen, L.; Chen, L.; Zhao, L.; Feng, J. Highly antifouling double network hydrogel based on poly-(sulfobetaine methacrylate) and sodium alginate with great toughness. *J. Mater. Sci. Technol.* **2021**, *85*, 235−244.
(30) Xiao, R.; Mai, T.-T.; Urayama, K.; Gong, J. P.; Qu, S. Micromechanical modeling of the multi-axial deformation behavior in double network hydrogels. *Int. J. Plast.* **2021**, *137*, No. 102901.
(31) Huang, X.; Li, J.; Luo, J.; Gao, Q.; Mao, A.; Li, J. Research progress on double-network hydrogels. *Mater. Today Commun.* **2021**, *29*, No. 102757.
(32) Chen, Q.; Zhu, L.; Zhao, C.; Wang, Q.; Zheng, J. A robust, one-pot synthesis of highly mechanical and recoverable double network hydrogels using thermoreversible sol-gel polysaccharide. *Adv. Mater.* **2013**, *25* (30), 4171−4176.
(33) Wang, Q.; Pan, X.; Wang, X.; Gao, H.; Chen, Y.; Chen, L.; Ni, Y.; Cao, S.; Ma, X. Spider web-inspired ultra-stable 3D Ti_3C_2TX (MXene) hydrogels constructed by temporary ultrasonic alignment and permanent in-situ self-assembly fixation. *Composites, Part B* **2020**, *197*, No. 108187.
(34) Hu, X.; Liang, R.; Li, J.; Liu, Z.; Sun, G. Mechanically strong hydrogels achieved by designing homogeneous network structure. *Mater. Des.* **2019**, *163*, No. 107547.
(35) Yang, J.; Fu, S.; Luo, F.; Guo, L.; Qiu, B.; Lin, Z. Homogeneous photoelectrochemical biosensor for microRNA based on target-responsive hydrogel coupled with exonuclease III and nicking endonuclease Nb.BbvCI assistant cascaded amplification strategy. *Mikrochim. Acta* **2021**, *188* (8), No. 267, DOI: 10.1007/s00604-021-04935-6.
(36) Postnova, I.; Sarin, S.; Zinchenko, A.; Shchipunov, Y. DNA−Chitosan Aerogels and Regenerated Hydrogels with Extroordinary Mechanical Properties. *ACS Appl. Polym. Mater.* **2022**, *4*, 663−671.
(37) Su, J.; Raabe, D.; Li, Z. Hierarchical microstructure design to tune the mechanical behavior of an interstitial TRIP-TWIP high-entropy alloy. *Acta Mater.* **2019**, *163*, 40−54.
(38) Wang, Y.; Xia, Y.; Xiang, P.; Dai, Y.; Gao, Y.; Xu, H.; Yu, J.; Gao, G.; Chen, K. Protein-assisted freeze-tolerant hydrogel with switchable performance toward customizable flexible sensor. *Chem. Eng. J.* **2022**, *428*, No. 131171.
(39) Gao, Y.; Jia, F.; Gao, G. Ultra-thin, transparent, anti-freezing organohydrogel film responded to a wide range of humidity and temperature. *Chem. Eng. J.* **2022**, *430*, No. 132919.
(40) Wang, Y.; Pang, B.; Wang, R.; Gao, Y.; Liu, Y.; Gao, C. An anti-freezing wearable strain sensor based on nanoarchitectonics with a highly stretchable, tough, anti-fatigue and fast self-healing composite hydrogel. *Composites, Part A* **2022**, *160*, No. 107039.

https://doi.org/10.1021/acsomega.3c05779
ACS Omega 2023, 8, 46676−46684